Thermal Oxidation of Porous Silicon: Study on Reaction Kinetics

Andrea Edit Pap,[†] Krisztián Kordás,[†] Thomas F. George,*[,‡] and Seppo Leppävuori[†]

Microelectronics & Materials Physics Laboratories, Department of Electrical and Information Engineering, EMPART Research Group of Infotech Oulu, University of Oulu, P.O. Box 4500, 90014-FIN Oulu, Finland, and Office of the Chancellor/Departments of Chemistry & Biochemistry and Physics & Astronomy, University of Missouri—St. Louis, St. Louis, Missouri 63121

Received: February 14, 2004; In Final Form: June 24, 2004

Porous silicon (PS) samples obtained by dark etching of p^+-type silicon wafers are oxidized in dry air, at various temperatures from 200 °C up to 800 °C for 1−20 h durations, to determine the kinetics of the reaction. The extent of oxidation calculated from mass gains is plotted as a function of oxidation time and temperature. By fitting the general reaction kinetic solutions of different-order reactions, one finds that the function valid for first-order kinetics gives the best matches. From the obtained reaction rates, the pre-exponential factors and activation energies of the oxidation process are determined using Arrhenius plots. It is found that, depending on the temperature range of the oxidation process, either one or two chemical reactions take place. At lower temperatures (200−400 °C), a reaction with an activation energy $E_{a,1} \approx 7$ kJ·mol^{-1} and a pre-exponential factor $A_1 \approx 0.2$ h^{-1} dominates. When the temperature is increased (400−800 °C), a second reaction starts, showing $E_{a,2} \approx 50$ kJ·mol^{-1} and $A_2 \approx 100$ h^{-1}.

Introduction

Because of the tunable optical properties of porous silicon (PS), PS has become a widely studied and applied material in recent years. A drawback of PS is its chemical reactivity. When stored in ambient air, the pore walls become partially oxidized, thus changing the refractive index, absorption coefficient, and luminescent properties of the material.[1,2] The room-temperature oxidation of PS is affected by a number of factors such as porosity of the samples, method used for drying after anodization, intensity of incident light, relative humidity, and so on.[3,4] To eliminate the problem of aging, for the stabilization of PS, a partial oxidation (pre-oxidation) is used in optical applications such as optical waveguides,[5,6] photodetectors,[7] dielectric filters,[8] and photoluminescent components.[9] While both dry and wet thermal oxidation processes have been investigated, all the details of the reaction kinetics of these processes have not been presented.[11−13] Therefore, the aims of this paper are to study how the thermal oxidation of porous silicon proceeds and to reveal the peculiarities of the reaction kinetics.

Experimental Methods

Free-standing porous silicon layers were manufactured by electrochemical dark etching of boron-doped (100) silicon wafers (0.015 Ω cm) in 8.8 M HF and 12 M C_2H_5OH electrolyte (i.e., 1.5:3.5 volume ratio of 50% HF and absolute ethanol). The constant anodization current densities were maintained using computer control. The electrolyte cell was made of PVDF.

In the first step, a porous layer was created, using either a 20 mA/cm^2 current density and 2140 s etching time (to form a lower porosity sample) or 65 mA/cm^2 current density and 840 s etching time (to obtain higher porosity). In the second step, the porous films were detached from the bulk by electrochemical polishing (330 mA/cm^2 for 50 s). After the process was complete, the samples were flushed in ethanol and stored in pentane. To calculate the porosity and thickness, control samples (anodized using the same conditions without detaching) were made and stripped in 1 M NaOH aqueous solution. The porosity was calculated as $p = (m_1 - m_2)/(m_1 - m_3)$, where m_1, m_2, and m_3 denote the mass of the original, anodized, and stripped wafer, respectively. The thickness of the formed PS layer was determined by profilometry after stripping. The porosity of the porous silicon membranes was either ∼70% (lower) or ∼83% (higher), and the thickness measured 30 μm. The oxidation procedure was carried out in air at various temperatures, from 200 °C up to 800 °C, for 1−20 h. Heating and cooling rates of 5 °C/min were applied to minimize the stress in the samples. Calculations of the extent of oxidation were based on gravimetric measurements (accuracy of 2%) of the samples.

Results and Discussion

When oxidizing the porous silicon layers in air, the silicon turns into SiO_2:

$$Si + O_2 \rightarrow SiO_2 \quad (1)$$

To calculate the oxide thickness growth rate in the spongy structure, the thicknesses of the walls between the pores were determined using field-emission scanning electron microscopy (FESEM) to analyze the non-oxidized porous silicon layers (Figure 1). The mean of the wall thicknesses was ∼30 nm. After 10 h at 800 °C, the whole structure was oxidized, yielding a rate of 0.025 nm/min, which is very close to the value of 0.02

* Corresponding author. E-mail: tfgeorge@umsl.edu.
[†] University of Oulu.
[‡] University of Missouri—St. Louis.

10.1021/jp049323y CCC: $27.50
Published on Web 08/04/2004

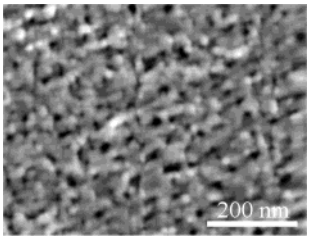

Figure 1. FESEM picture of a pristine porous silicon layer. The structure consists of 10−40 nm diameter holes confined by Si walls with a mean thickness of ∼30 nm.

nm/min published for dry thermal oxidation of bulk silicon at 800 °C.[14]

The extent of oxidation (ox) is defined by the ratio of oxygen built in (n_{O_2}) and the initial silicon amount (n_{Si}), and it is measured via the mass gain ($m_t - m_0$):

$$\mathrm{ox} = \frac{n_{SiO_2}}{n_{Si}} = \frac{n_{O_2}}{n_{Si,0}} = \frac{m_t - m_0}{m_0}\frac{M_{Si}}{M_{O_2}} \qquad (2)$$

where M_{O_2} and M_{Si} are the molar masses of oxygen and silicon, respectively. Because the initial amount of Si changes considerably during the heating/cooling steps (the ox ≠ 0 values at $t = 0$ show the extent of oxygen taken up within the heating and cooling ramps; see Figure 2a), the measurement data have been corrected to eliminate the amount of SiO_2 formed in the transient species (i.e., at $t = 0$, there is no SiO_2 in the structure) as

$$\mathrm{ox}^* = \frac{n^*_{O_2}}{n^*_{Si,0}} = \frac{n_{O_2} - \mathrm{ox}_0 \cdot n_{Si,0}}{(1 - \mathrm{ox}_0) n_{Si,0}} \qquad (3)$$

With these corrections, the oxidation which took place at constant temperature could be revealed (Figure 2b).

In both parts of Figure 2, saturation curves are seen. At 200 and 400 °C, the oxidation saturates to 0.16 and 0.33, respectively. At higher temperatures, the oxidation is faster, and the achieved SiO_2 concentrations are much higher compared to the corresponding lower temperature measurements. At 800 °C, the oxidation saturates to 1 (i.e., the entire amount of PS turns into porous SiO_2 within 10 h). Although the curve for 600 °C shows a monotonic increase with time, saturation could not be observed because of the short time frame.

The results suggest that more reactions are occurring within the oxidation process. The similar, multistep character of the oxidation process had been found in the case of selective (laser-assisted) oxidation of metals.[15−17] At lower temperatures (200−400 °C), a reaction with low activation energy dominates. The saturation to a low oxide content is explained with the limited amount of reactive sites on the pore walls. At 600 and 800 °C, other reactions with higher activation energies are enabled because of the high thermal energy of the reactants. In the case of ∼83% porosity and 30-μm-thick porous silicon membranes, similar results were obtained. However, because of the larger specific surface area with more high-energy reaction centers on the surface, oxidation is faster and shows higher saturation for lower temperatures, compared to the PS membranes with 70% porosity. Similar results (i.e., partial oxidation) were obtained by others[13] when oxidizing PS at lower temperatures. In comparison to our results, the saturation is complete at ∼40%, probably because of the different orientation (111) and lower impurity concentration of the Si wafers used.

To determine the chemical reaction kinetics of oxidation, general reaction kinetic solutions of different-order reactions (first- and second- as well as third-order)[18] were fitted to the experimental results, and the first-order kinetics

$$\mathrm{ox}^* = 1 - \mathrm{e}^{-kt} \qquad (4)$$

showed the best fits to the ox*(T,t) data. The fitting parameter k defines the reaction rate coefficients of chemical reactions at given temperatures. By plotting ln$k$ as a function of $-(RT)^{-1}$ (Figure 3), one can obtain the activation energies E_a's and collision rates A's for the reactions from the Arrhenius law (eq 5):

$$k = A \cdot \mathrm{e}^{-E_a/RT} \qquad (5)$$

The nonlinearity of the Arrhenius plots supports the presumption concerning the existence of two types of oxidation mechanisms. Therefore, two linear functions were fitted to both graphs in Figure 3: one over the points representing the temperatures 200, 400, and 600 °C and the other for the temperatures 400, 600, and 800 °C. The as-obtained slopes give the activation energies for the reactions going on at the given temperature ranges (Table 1).

The activation energies obtained show variation with the porosity: the higher the porosity, the lower the activation energy of the oxidation for both reactions. This can be explained by the higher stress formed in the Si lattice for the higher porosity samples, which is known to enhance oxidation for most metals.

Because of the large deviation of the pre-exponential constants (∼50% in the fitting), it was not possible to find any characteristic variation of the collision rate with the porosity. For both levels of porosity, the average collision numbers were ∼0.2 and ∼100 h^{-1} for the reactions with lower and higher activation energies, respectively.

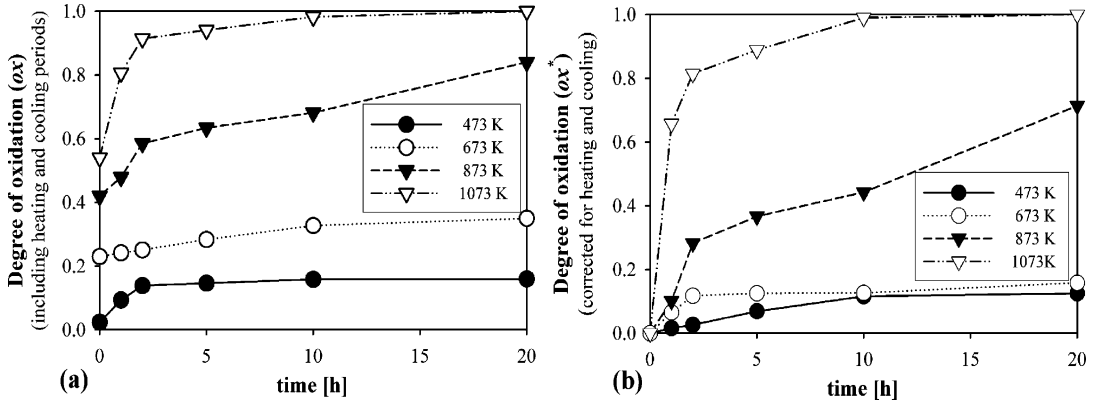

Figure 2. Oxidation extent of 70% porosity and 30 μm thick porous membranes versus time and temperature (a) as measured and (b) corrected for the amount of oxide formed during the heating and cooling periods.

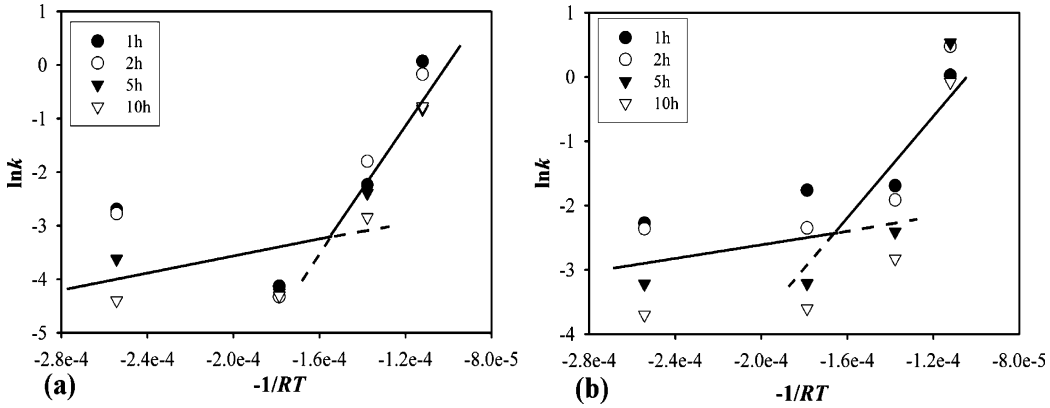

Figure 3. Arrhenius plots of the thermal oxidation reaction rates of PS with porosities of (a) 70% and (b) 83%.

TABLE 1: Apparent Mean of Activation Energies for the Oxidation

porosity	$E_{a,1}$ (kJ·mol^{-1})	$E_{a,2}$ (kJ·mol^{-1})
70%	8.3 ± 3.5	55.1 ± 6.3
83%	5.4 ± 1.4	44.6 ± 7.2

The reaction with low activation energy and collision number represents the oxidation of the pore walls. This is the reaction path which is probably most responsible for the aging of PS samples stored in air. It is very similar to the formation of a native oxide layer on bulk wafers (i.e., it stops when a layer thickness of ~2 nm is reached because the reaction becomes diffusion-limited). The second reaction, with considerably higher activation energy, is related to the oxidation of the bulk of the Si skeleton. In this case, the increased activation energy is due to the additional energy needed for the diffusion of oxygen through the oxide layer toward the SiO_2/Si interface. Differential scanning calorimetry studies on the low-temperature oxidation (25−350 °C) of PS also revealed two reaction routes, although the published activation energies were significantly higher (53 and 134 kJ·mol^{-1}).[12]

The activation energies for PS oxidation obtained here (Table 1) as well as the data published by others are considerably lower than the values published in the literature for the bulk material (154 kJ·mol^{-1} for dry[14] and 119−126 kJ·mol^{-1} for wet[19] oxidation). The higher reactivity of porous silicon structures compared to pristine wafers is explained by nanosize effects arising from the irregularities of the surface, as the local density of states shows variation with the positions of the surface atoms.[20] As a macroscopic behavior, it was demonstrated with the Kelvin probe method that surface potentials measured on PS and Si differ significantly,[21,22] so that the redox properties of the porous and pristine surfaces are different.[23,24] In addition, other factors such as residual stresses and chemical impurities remaining after anodization could enhance the oxidation.[2]

The low-temperature (T < 800 °C) oxide growth rates obtained for porous silicon were considerably higher than those for bulk Si. The oxidation of bulk Si is well described by the Deal−Grove linear-parabolic growth law $x^2 + Ax = B(t + \tau)$, where x is the oxide thickness grown within the period of time t. The symbols A, B, and τ are temperature-dependent rate constants.[25,26] For T < 800 °C, the law simplifies to a linear form, and the rate is given by the B/A quotient. Because B/A shows exponential decay with decreasing temperature, the calculated growth rate for 600 °C becomes ~0.001 nm/min, which is considerably lower than the value of ~0.01 nm/min for PS approximated from our experimental results. While considerable oxidation of the porous silicon samples occurs at 400 and 200 °C within a few hours in air, practically no oxidation of Si takes place within such a short period.[25−27]

Conclusions

This work has dealt with the dry thermal oxidation of free-standing porous silicon films. The oxidation shows first-order kinetics and is found to be dependent on the porosity of PS membranes. Depending on the temperature range of the process only, either one or two independent chemical reactions take place. At lower temperatures, the oxidation of the porous surfaces is enabled via a reaction with $E_a = 8.3 \pm 3.5$ kJ·mol^{-1} and $A = 0.2$ h^{-1} (for a 70% porosity sample) or $E_a = 5.4 \pm 1.4$ kJ·mol^{-1} and $A = 0.2$ h^{-1} (for 83% porosity). As the temperature increases above 400 °C, a second reaction with considerably higher activation energy begins (55.1 ± 6.3 and 44.6 ± 7.2 kJ·mol^{-1} at 70% and 83% porosity, respectively).

Acknowledgment. Financial support of the Graduate School of Infotech Oulu is acknowledged. A.E.P. acknowledges the grants given by Tauno Tönningin Säätiö, Oulun Yliopiston Tukisäätiö, Naisten Tiedesäätiö, and Tekniikan Edistämissäätiö. K.K. is grateful for the Nokia Visiting Scholarship received from the Nokia Foundation.

References and Notes

(1) Kim, D. A.; Lee, J. S.; Park, M. B.; Cho, N. H. *J. Korean Phys. Soc.* **2003**, *42*, 184.

(2) Bisi, O.; Ossicini, S.; Pavesi, L. *Surf. Sci. Rep.* **2000**, 38.

(3) Petrova, E. A.; Bogoslovskaya, K. N.; Balagurov, L. A.; Kochoradze, G. I. *Mater. Sci. Eng., B* **2000**, *69*−*70*, 152.

(4) Salonen, J.; Lehto, V.-P.; Laine, E. *Appl. Surf. Sci.* **1997**, *120*, 191.

(5) Maiello, G.; LaMonica, S.; Ferrari, A.; Masini, G.; Bondarenko, V. P.; Dorofeev, A. M.; Kazuchits, N. M. *Thin Solid Films* **1997**, *297*, 311.

(6) Carrier, J.; Lupi, C.; Haji, L.; Boisrobert, C. *Mater. Sci. Semicond. Process.* **2000**, *3*, 357.

(7) Lee, M. K.; Tseng, Y. C.; Chu, C. H. *Appl. Phys. A* **1998**, *67*, 541.

(8) Berger, M. G.; Arnes-Fisher, R.; Thönissen, M.; Krüger, M.; Billat, S.; Lüth, H.; Hilbrich, S.; Theiss, W.; Grosse, P. *Thin Solid Films* **1997**, *297*, 237.

(9) Tsybeskov, L.; Duttagupta, S. P.; Fauchet, P. M. *Solid State Commun.* **1995**, *95*, 429.

(10) Park, J. Y.; Lee, J. H.; Sim, J. H.; Cho, C. S.; Bae, Y. H. *J. Korean Phys. Soc.* **2002**, *41*, 160.

(11) Koyama, H.; Fauchet, P. M. *Appl. Phys. Lett.* **2000**, *77*, 2316.

(12) Salonen, J.; Lehto, V.-P.; Laine, E. *J. Porous Mater.* **2000**, *7*, 335.

(13) Xu, D.; Guo, G.; Gui, L.; Tang, Y.; Zhang, B. R.; Qin, G. G. *J. Appl. Phys.* **1999**, *86*, 2066.

(14) Jimin, W.; Yu, L.; Ruiwei, L. *Solid-State Electron.* **2003**, *47*, 1699.

(15) Hevesi, I.; Nánai, L.; Vajtai, R. *Superlattices Microstruct.* **1987**, *3*, 409.
(16) Nánai, L.; Vajtai, R.; Kovács, I.; Hevesi, I. *J. Less-Common Met.* **1989**, *152*, L23.
(17) Nánai, L.; Vajtai, R.; Hevesi, I.; Laiho, R.; Heikkilla, L. *Superlattices Microstruct.* **1992**, *11*, 435.
(18) Atkins, P. W.; de Paula, J. *Physical Chemistry*; Oxford University Press: Oxford, U.K., 2002.
(19) Ligenza, J. R. *J. Phys. Chem.* **1961**, *65*, 2011.
(20) Alfonso, D.; Wu, S.-Y.; Jayanthi, C. S.; Kaxiras, E. *Phys. Rev. B* **1999**, *59*, 7745.
(21) Mizsei, J. *Vacuum* **2002**, *67*, 59.
(22) Mizsei, J.; Shrair, J. A.; Zólomy, I. *Appl. Surf. Sci.*, in press.
(23) Ott, N.; Nerding, M.; Müller, G.; Brendel, R.; Strunk, H. P. *J. Appl. Phys.* **2004**, *95*, 497.
(24) Pap, A. E.; Kordás, K.; Peura, R.; Leppävuori, S. *Appl. Surf. Sci.* **2002**, *201*, 56.
(25) Deal, B. E.; Grove, A. S. *J. Appl. Phys.* **1965**, *36*, 3770.
(26) Harrison, H. B.; Dimitriev, S. *Microelectron. J.* **1991**, *22*, 3.
(27) Revesz, A. G.; Hughes, H. L. *J. Non-Cryst. Solids* **2003**, *328*, 48.